DOI: 10.1002/ejic.200600990

Study of the Defects in Sintered SnO_2 by High-Resolution Transmission Electron Microscopy and Cathodoluminescence

David Maestre,[a] Julio Ramírez-Castellanos,[b] Pedro Hidalgo,[a] Ana Cremades,[a] José M. González-Calbet,[b] and Javier Piqueras*[a]

Keywords: Semiconductors / Luminescence / Microstructure / Resistivity

The defect structure of sintered SnO_2 was investigated by high-resolution transmission electron microscopy (HRTEM), cathodoluminescence (CL), and electrical measurements. HRTEM shows the presence of the SnO phase in the sintered samples as well as twinning, stacking faults, and disordered intergrowths. The sintered samples annealed under an oxygen atmosphere show changes in the defect structure and in the CL spectra. In particular, the intensity of a CL band at 1.94 eV, related to oxygen vacancies, decreased as the electrical resistivity increased. The results are discussed by considering the presence of stoichiometric defects such as oxygen vacancies and Sn interstitials in the final structure and their evolution during the annealing process under an oxygen atmosphere.

Introduction

SnO_2 is a semiconducting oxide of interest for technological applications such as gas sensors, transparent electrical contacts, or optoelectronics.[1–3] It is commonly accepted that its electrical conductivity is related to its nonstoichiometry, which is due to a large concentration of oxygen vacancies that act as shallow donors close to the conduction band.[4] However, this vacancy model seems to raise a few fundamental questions with regard to the general understanding of the phenomenon of transparent conductivity. Some theoretical results[5] point to an important role of the interstitial Sn atoms, which present unusual stability owing to the multivalence of tin, under different chemical potential conditions in SnO_2.

In this work, the defect structure of sintered SnO_2 ceramic samples and its correlation with optical and electrical properties were investigated. In particular, the role of oxygen vacancies and of tin interstitials in the luminescence and electrical resistivity of the sintered samples was analyzed. Samples prepared under different thermal treatments were characterized by the cathodoluminescence (CL) mode in a scanning electron microscope (SEM), x-ray diffraction (XRD), high-resolution transmission electron microscopy (HRTEM), and electrical resistivity measurements.

[a] Departamento de Física de Materiales, Facultad de Ciencias Físicas, Universidad Complutense de Madrid,
28040 Madrid, Spain
Fax: +34-91-394-4547
E-mail: piqueras@fis.ucm.es
[b] Departamento de Química Inorgánica, Facultad de Ciencias Químicas, Universidad Complutense de Madrid,
28040 Madrid, Spain

Results

The sintered samples have irregular-shaped grains with different sizes and porosities as a function of the annealing temperature. We have previously reported[6] that the cathodoluminescence spectra of SnO_2-sintered samples show three main contributions centered around 1.94, 2.25, and 2.58 eV, whose relative intensities depend on the sintering treatment. The 1.94 eV emission has been related to the presence of oxygen vacancies[6,7] which act as shallow donors in SnO_2.

Figure 1 shows CL spectra recorded at 80 K on samples sintered in air for 10 h at 1200 °C, and subsequently treated under an oxygen atmosphere at 600 and 900 °C. As a reference, the spectrum of the sample sintered in air for 10 h at 1200 °C, is also represented. No significant changes in the spectrum can be appreciated after the treatment under an oxygen atmosphere at 600 °C. However, thermal treatments at higher temperatures (900 °C) produce a decrease in the total CL signal, but mainly of the 1.94 eV emission intensity. Figure 2 shows CL spectra of samples sintered in air for 10 h at 1500 °C, with and without subsequent treatment in an oxygen atmosphere. The 2.25 eV emission is dominant in the three spectra, whereas the 1.94 eV emission has almost disappeared. A decrease in the CL intensity is also observed as the temperature of the oxygen annealing is increased.

In order to investigate the changes that these treatments produce in the oxide microstructure and composition of SnO_2, analysis by means of XRD and HRTEM were carried out. XRD of the samples sintered at 1200 °C and 1500 °C show a crystalline structure of rutile type, with a tetragonal unit cell and parameters a = 0.4738 nm and c =

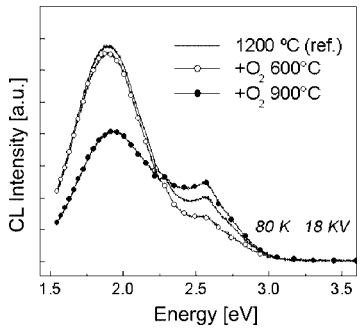

Figure 1. CL spectra of samples sintered in air at 1200 °C, some of which were subsequently treated under an oxygen atmosphere at 600 or 900 °C.

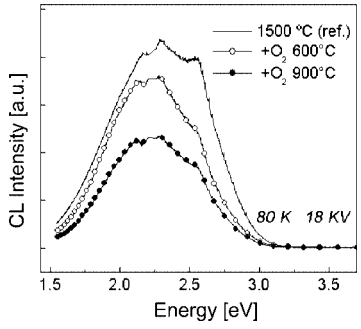

Figure 2. CL spectra of samples sintered in air at 1500 °C for 10 h, and samples further annealed under an atmosphere of oxygen at 600 and 900 °C.

0.3187 nm, and $P4_2/mnm$ space group. SAED and HRTEM studies show the presence of different defects, including twinning, stacking faults, disordered intergrowths, domains, and amorphization.

Figure 3a shows the fast Fourier transform (FFT) pattern along the [001] zone axis of the sample sintered at 1200 °C, which can be indexed on the basis of the rutile crystal structure. The corresponding HRTEM image (Figure 3b) shows a very well-ordered material with interplanar distances of 0.47 nm.

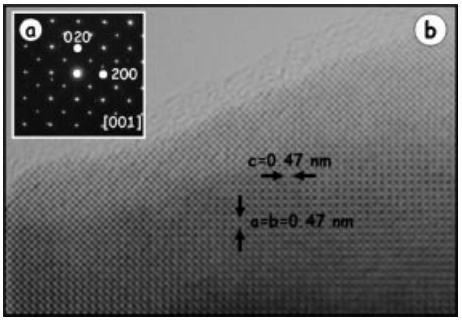

Figure 3. FFT pattern along the [001] axis (a), and HRTEM image (b) of a sample sintered in air at 1200 °C for 10 h.

In contrast, Figure 4a shows the FFT pattern along the [111] zone axis of the same sample, which can also be indexed on the basis of the rutile crystal structure. However, the splitting of the main diffraction spots (marked by arrows) suggests the existence of twining. In the corresponding HRTEM image (Figure 4b), twin planes along (011) are observed. These straight twin boundaries are coherent and consist of Sn atoms shared by the two neighboring components of the twin.[8] Huang et al.[9] reported that the Sn sublattice is mirror symmetric to the coherent twin boundary (CTB), whereas the oxygen atoms forming octahedral cages around the Sn atoms are not mirror symmetric to the CTB.

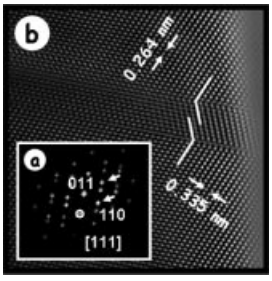

Figure 4. FFT pattern along the [111] zone axis (a) of a sample sintered in air at 1200 °C for 10 h and the corresponding HRTEM image (b), showing twin planes along (011).

Figure 5 corresponds to a different area of the same sample. The inset (Figure 5a) shows the corresponding FFT pattern along the [111] zone axis, which shows both splitting and streaking of the diffraction spots; this is indicative of high structural disorder, as it can be seen in the corresponding HRTEM micrograph (Figure 5b) where recurrent twinning and disorder intergrowths are observed. HRTEM characterization also shows that after annealing under an oxygen atmosphere at 900 °C, the density of defects decreases.

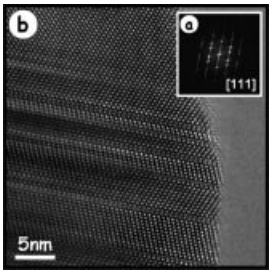

Figure 5. FFT pattern along the [111] axis (a) and HRTEM image showing structural disorder and recurrent twinnings (b) corresponding to a different area of the sample observed in Figures 3 and 4.

Alternatively, Figure 6a shows the SAED pattern of the sample treated at 1500 °C in air for 10 h. The diffuse rings indicate the presence of an amorphous phase. Moreover, the intensity and discrete spots in this FFT pattern (Figure 6b) suggest the presence of randomly oriented grains of very small dimensions. Figure 6c reveals a complex microstructure, where crystallized domains (dashed circle) in an amorphous matrix are observed. Therefore, in some crystals of this sample, interplanar distances of 0.48 nm were measured (Figure 7a), which corresponds to the *c* axis of the SnO phase. The inset (Figure 7b) shows the corresponding

FFT pattern. Notably, further thermal treatment at 900 °C under an oxygen atmosphere led to better recrystallization of the sample.

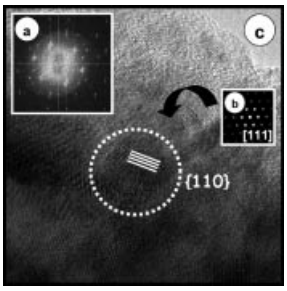

Figure 6. SAED (a) and FFT pattern (b) of a sample sintered in air at 1500 °C for 10 h. HRTEM image (c) reveals the presence of crystallized domains in an amorphous matrix.

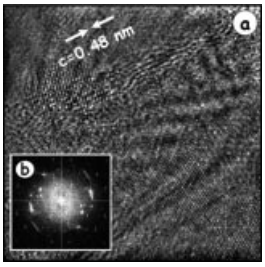

Figure 7. HRTEM image (a) of a sample sintered in air at 1500 °C for 10 h. The inset shows the corresponding FFT pattern.

As the presence of oxygen vacancies acting as donors determines the electrical properties of SnO_2, resistivity measurements were carried out. Results are presented in Table 1 and Figure 8.

Table 1. Evolution of the samples resistivity as a function of the sintering temperature and post annealing under an oxygen atmosphere at 900 °C.

Temperature [°C]	Resistivity [Ω cm]	+ O_2 (900 °C)
1000	$(0.9 \pm 0.2)\ 10^3$	$(3.1 \pm 0.5)\ 10^4$
1100	$(3.5 \pm 0.7)\ 10^3$	
1200	$(2.3 \pm 0.4)\ 10^4$	$(1.2 \pm 0.2)\ 10^4$
1300	$(9.0 \pm 1.5)\ 10^5$	

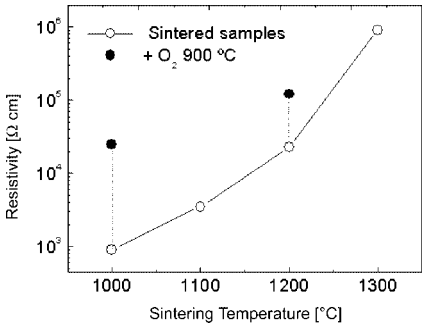

Figure 8. Resistivity of samples as a function of the sintering temperature and further annealing under an oxygen atmosphere at 900 °C.

The results show a rise in the resistivity as the temperature used during the sintering treatments was increased. Note that the *y* axis in Figure 8 is logarithmic-scaled, which denotes a faster increase in the resistivity at higher sintering temperatures. Moreover, the annealing process, which is performed under an oxygen atmosphere heated at 900 °C, also causes an increase in the resistivity, as shown in Figure 8. The samples sintered at temperatures above 1300 °C present a resistivity higher than $10^8\ \Omega$cm, but exact values could not be obtained with the experimental setup used.

Discussion

The influence of oxygen vacancies (V_O) on the electrical conduction, structure, or luminescence properties of SnO_2 has been often considered, whereas the influence of Sn interstitials (Sn_i) is usually ignored. Different authors[4,10] have pointed out that oxygen vacancies are mainly responsible for several optical and electrical properties of SnO_2, and they act as shallow donor levels below the conduction band. Both donor defects, V_O and Sn_i, can donate electrons to the conduction band without increasing the optical interband absorption, which explains the coexistence of conductivity and transparency in this material. Themlin et al.,[11] from their synchrotron results on the SnO_2 (110) surface, concluded the existence of states sensitive to oxygen chemisorption, situated 1.4 eV above the valence band top. These levels, related to the Sn^{2+} cation and associated with the presence of oxygen vacancies, are compatible with the transitions leading to the 1.94 eV emission observed in the present work. Also, our previous studies[6] showed the connection between this emission and the oxygen vacancies. The fact that treatment of the sample under an oxygen atmosphere heated at 900 °C causes the intensity of the 1.94 eV band to decrease, also indicates an annealing-induced decrease in the vacancy concentration as a result of thermally activated oxygen diffusion. In the samples sintered at 1500 °C without additional treatments, the 1.94 eV CL emission hardly appears; therefore, subsequent oxygen treatments cannot affect this emission intensity as much as in the samples sintered at 1200 °C. The kinetics of the oxygen–SnO_2 reaction, as well as the oxygen diffusion mechanism, were previously investigated. Kamp et al.[12] concluded that at temperatures below 800 °C, only surface reactions like adsorption occurs, which is the diffusion process that is activated at higher temperatures. These processes would be related to a change in the oxidation state of the adsorbed oxygen at 450 °C,[13] which turns O_2^- into O^- (the latter being more reactive). Themlin et al.[11] observed that an increase in the temperature to 630 °C initiates the bulk-oxygen diffusion process. Our CL results (Figure 1) show a decrease in the 1.94 eV emission, related to the oxygen vacancies, that occurs during the treatment of the sample under an oxygen atmosphere heated at 900 °C, which agrees with these observations. Sintering at high temperatures, up to 1500 °C, results in the progressive disappearance of the oxygen vacancies' concentration, as suggested not only by

the decrease in the 1.94 eV emission, but also for the charge effects appearing during the observations in SEM. The resistivity increase that is produced at higher sintering temperatures and during oxygen treatments, shown in Figure 8, agrees with a decrease in the vacancy concentration detected by the evolution of the 1.94 eV band. Indeed, perfectly stoichiometric samples are highly resistive.[14] Paria et al.[15] obtained similar resistivity results on sintered SnO_2 to those presented here. The crystallinity improvement produced by the oxygen treatments agrees with the well-ordered appearance observed in the HRTEM images. Conversely, sintering treatments can also increase the presence of defects (as shown in Figures 5 and 7), which reduces the carriers mobility, and the conductivity as well. Previous work confirms the decrease in the conductivity as the pressure and the oxygen content in the reactive atmosphere is increased.[16]

SAED and HRTEM analyses show that planar defects, such as recurrent twinning, stacking faults, and vacancies, are present in these samples. In addition, at high temperatures, the material seems to consist of both a polycrystalline SnO_2 phase and an amorphous SnO phase.[17] Moreover, the decomposition of SnO_2 into SnO, according to the reaction $SnO_2 \rightarrow SnO + V_O^-$, at high temperatures, has to be considered. These processes begin with the formation of intermediate phases, such as Sn_3O_4, SnO, and even metallic Sn, by internal oxygen disproportionate allocation, depending on the temperature and atmosphere conditions, as described by Cahen et al.[18] Many crystal defects, including twinning, crystallographic shear planes (CSP), stacking faults, and oxygen vacancies, are formed during these processes. In our case, the partial SnO formation was observed when the SnO_2 material was treated at high temperatures in air. Because both compounds are structurally related, it is reasonable to think that they can easily exist in the same crystal, as observed in samples treated at 1500 °C in air (Figure 7). In the SnO_2 rutile structure, each Sn atom has six oxygen neighbors, which form a distorted octahedral. The distance between the Sn and O atoms within one octahedron is 0.21 nm. In SnO, each Sn atom has four oxygen neighbors, but all of them are located on the same side of the Sn atoms, as shown by the pyramid consisting of one Sn atom and four O atoms in the SnO unit cell. The Sn–O bonds have a length of 0.222 nm. Accordingly, the SnO_2 phase can be easily transformed into the SnO phase by removing the O atoms from SnO_2 and by slightly adjusting the position of the Sn atoms. The formation of Sn_i requires the rearrangement of its atomic environment by ionic relaxations resembling the local structure of SnO, which can also explain the observed SnO phase.

The sintered samples that were treated under an oxygen atmosphere were found mainly to consist of the SnO_2 phase. This shows that the SnO phase formed by the reduction of SnO_2 at high temperature is unstable under oxidation conditions and will be transformed into the SnO_2 rutile phase through an oxidation process. During this process, a decrease in the V_O and Sn_i concentration takes place along with an increase in resistivity.

Conclusions

Sintering SnO_2 in air at high temperatures results in a high density of defects, as observed by SAED and HRTEM, as well as in the presence of the SnO phase which can be explained by Sn_i formation. The sintering treatments modify the CL signal, mainly the 1.94 eV emission, which disappears at temperatures greater than 1500 °C. This emission, which has been associated with the presence of oxygen vacancies, is decreased during post sintering treatments under an oxygen atmosphere. This process governed by oxygen diffusion, was detected after treatments at 900 °C. The decrease in the V_O concentration is associated with a large increase in resistivity. Annealing under an oxygen atmosphere at high temperatures improves the crystallinity of the samples and leads to the formation of a pure SnO_2 rutile phase.

Experimental Section

The starting material used was commercial SnO_2 powder (Aldrich Chemical Company Inc., 99.9% purity). The powder, consisting of particles and aggregates of rounded particles with sizes of about 200 nm, was compacted under a compressive load of 2 tons to form disc-shaped samples that were about 7 mm in diameter and 2 mm thick. The samples were sintered in air for 10 h at temperatures between 1000 °C and 1500 °C and some of them were subsequently annealed for 2 h under an oxygen atmosphere at 600 °C and 900 °C.

The samples were observed in the secondary electron (SE) and cathodoluminescence (CL) modes with a Hitachi S-2500 or a Leica 440 SEM, at accelerating voltages ranging from 10 to 30 kV at a temperature of 80 K. The CL spectra were recorded either with the photomultiplier tube attached to an Oriel 78215 computer-controlled monochromator or with a CCD camera with a built-in spectrograph (Hamamatsu PMA-11). Resistivity measurements were performed by means of the Van der Pauw technique, in air and at room temperature. Structural information of the samples was obtained by X-ray diffraction (XRD) performed with a Philips diffractometer and high resolution transmission energy microscopy (HRTEM) with a JEOL 300 FEG electron microscope.

Acknowledgments

This work was supported by MEC (project MAT 2003-00455) and by UCM-CM (Group 910146).

[1] B. Drevillon, S. Kumer, P. R. Carbarrocas, J. M. Siefert, *J. Appl. Phys. Lett.* **1989**, *54*, 2088.
[2] G. Martinelli, M. C. Carotta, E. Traversa, G. Ghiotti, *MRS Bull.* **1999**, *24*, 30.
[3] A. Lousa, S. Gimeno, J. Marti, Vacuum **1994**, *45*, 1143.
[4] D. F. Cox, T. B. Fryberger, S. Semacik, *Phys. Rev. B* **1988**, *38*, 2072.
[5] C. Kiliç, A. Zunger, *Phys. Rev. Lett.* **2002**, *88*, 095501.
[6] D. Maestre, A. Cremades, J. Piqueras, *J. Appl. Phys.* **2003**, *95*, 3027.
[7] D. Maestre, A. Cremades, J. Piqueras, *Semicond. Sci. Technol.* **2004**, *19*, 1236.
[8] J. G. Zheng, X. Pen, M. Scheweizer, F. Zhou, U. Weimar, W. Gopel, M. Ruhle, *J. Appl. Phys.* **1996**, *79*, 7688.

[9] J. Y. Huang, B. H. Park, D. Jan, X. Q. Pan, Y. T. Zhu, Q. X. Jia, *Philos. Magn. A* **2002**, *82*, 735.
[10] S. Samson, C. G. Fonstad, *J. Appl. Phys.* **1973**, *44*, 4618.
[11] J. M. Themlin, R. Sporken, J. Darville, R. Caudano, J. M. Gilles, R. L. Johnson, *Phys. Rev. B* **1990**, *42*, 11914.
[12] B. Kamp, R. Merkle, J. Maier, *Sens. Actuators, B* **2001**, *77*, 534.
[13] U. Pulkkinen, T. T. Rantala, T. S. Rantala, V. Lantto, *J. Mol. Catal. A* **2001**, *166*, 15.
[14] C. Terrier, J. P. Chatelon, R. Berjoan, J. A. Roger, *Thin Solid Films* **1995**, *263*, 37.
[15] M. K. Paria, H. S. Maiti, *J. Mater. Sci.* **1983**, *18*, 2101.
[16] B. Sterjna, C. G. Granqviest, A. Seidel, L. Häggström, *J. Appl. Phys.* **1990**, *68*, 6241.
[17] Z. W. Chen, J. K. L. Lai, C. H. Shek, *J. Solid State Chem.* **2005**, *178*, 892.
[18] S. Cahen, N. David, J. M. Fiorani, A. Maitre, M. Vilasi, *Thermochim. Acta* **2003**, *403*, 275.

Received: October 20, 2006
Published Online: March 2, 2007

